Substrate Integrated Waveguide (SIW) Leaky-Wave Antenna With Transverse Slots

Juhua Liu, David R. Jackson, *Fellow, IEEE*, and Yunliang Long, *Senior Member, IEEE*

***Abstract*—A novel slotted substrate integrated waveguide (SIW) leaky-wave antenna is proposed. This antenna works in the TE_{10} mode of the SIW. Leakage is obtained by introducing a periodic set of transverse slots on the top of the SIW, which interrupt the current flow on the top wall. It is seen that three modes (a leaky mode, a proper waveguide mode, and a surface-wave-like mode) can all propagate on this structure. The wavenumbers of the modes are calculated theoretically and are numerically evaluated by HFSS simulation. The leakage loss, dielectric loss, and conductor loss are also analyzed. A uniform slotted SIW leaky-wave antenna is designed that has good beam scanning from near broadside (though not exactly at broadside) to forward endfire. This type of SIW leaky-wave antenna has a wide impedance bandwidth and a narrow beam that scans with frequency. Measured results are consistent with the simulation and the theoretical analysis.**

***Index Terms*—Leaky wave, leaky-wave antenna, periodic structure, SIW, substrate integrated waveguide, surface wave.**

I. Introduction

THE TRANSVERSE slotted rectangular waveguide [1] is a simple structure that works as a leaky-wave antenna having frequency beam-scanning capability, with an orthogonal polarization from the conventional traveling-wave slotted antenna [2]. Because of the polarization, the transverse slotted rectangular waveguide can scan from near broadside to endfire if the waveguide is filled with a dielectric material [3].

However, rectangular waveguide is costly, heavy, and bulky. Substrate integrated waveguide (SIW) has been recently investigated [4]–[9] for its significant advantages such as low cost, low loss, and easy integration with planar circuits. It consists of a wide microstrip line that is shorted at the edges with conductive vias, acting as a rectangular waveguide. The SIW has been widely developed for integrated microwave and millimeter-wave components and antennas.

Several types of SIW leaky-wave antennas have been proposed recently [10]–[16]. The SIW leaky-wave antennas published in [10] and [11] utilize leakage due to the periodic gaps between the vias with sufficiently large period. This leaky-wave antenna radiates from the side-walls of the SIW. The half-mode SIW leaky-wave antenna discussed in [12] is similar to the half-width Menzel leaky-wave antenna in microstrip line [17], which has leakage from the open edges of the microstrip line. An SIW leaky-wave antenna with a long slot was investigated in [13], and low sidelobes were obtained. In these cases [10]–[13], it is difficult to achieve endfire radiation due to the polarization of the radiating equivalent magnetic currents. The composite right/left-handed SIW leaky-wave antennas proposed in [14] and [15] have beam scanning from the backward to the forward region. An SIW leaky-wave antenna with a series of inclined slots [16] can produce different polarizations depending on the input port. The half-mode SIW transverse slot array antenna in [18] is not used as a leaky-wave antenna and radiates mainly at broadside. The SIW slot array antenna in [19] has a wide bandwidth, a broad beamwidth, and a high gain, but this antenna is also not a leaky-wave antenna and does not have a scanning ability.

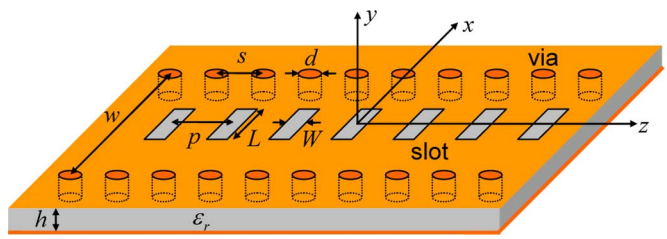

Fig. 1. Geometry of the slotted SIW leaky-wave antenna. The SIW has $w = 10.5$ mm, $\varepsilon_r = 2.25$, $h = 1$ mm, $d = 0.8$ mm, and $s = 1.6$ mm. The slots have $L = 4.55$ mm, $W = 0.45$ mm, and $p = 2.5$ mm.

In this paper, we propose a novel leaky-wave antenna based on SIW. The proposed SIW leaky-wave antenna, shown in Fig. 1, not only maintains the advantages of transverse slotted rectangular waveguide, but also has the advantages of SIW including low cost and ease of fabrication. This antenna has a simple structure and is easy to feed with a microstrip line. This antenna works in the TE_{10} mode of the SIW. Leakage is obtained by introducing a periodic set of centered transverse slots on the top of the SIW, which interrupt the current flow on the top wall. This antenna scans in the forward quadrant as frequency changes. Because of the polarization, it can radiate well at endfire when an infinite (or large) ground plane is present. (However, it is difficult to obtain a beam radiating at exactly endfire if a finite ground plane is used due to finite ground diffraction effects.)

Since the transverse slotted SIW antenna works similarly as a transverse slotted rectangular waveguide, we analyze this

Manuscript received August 16, 2010; revised March 17, 2011; accepted April 04, 2011. Date of publication September 15, 2011; date of current version January 05, 2012. This work was supported by the Natural Science Foundation of China (61172026), the Research Program of Guangzhou (2010Y1-C401), and NSFC-Guangdong (U0935002).

J. Liu and Y. Long are with the Department of Electronics and Communication Engineering, Sun Yat-sen University, Guangzhou 510275, China (e-mail: liujuhua_2000@hotmail.com; isslyl@mail.sysu.edu.cn).

D. R. Jackson is with the Department of Electrical and Computer Engineering, University of Houston, Houston, TX 77204-4005 USA (e-mail: djackson@uh.edu).

Color versions of one or more of the figures in this paper are available online at http://ieeexplore.ieee.org.

Digital Object Identifier 10.1109/TAP.2011.2167910

structure based on the theory of a transverse slotted rectangular waveguide [3]. A leaky (improper) waveguide mode, a proper waveguide mode, and a surface-wave-like mode can all propagate in the transverse slotted SIW antenna just as in the transverse slotted rectangular waveguide. In a leaky-wave antenna, the wavenumber is the key to determine the radiation characteristics. We calculate the wavenumber theoretically and by using HFSS simulation. The leakage loss, dielectric loss, and conductor loss are also analyzed. The radiation efficiency is then found theoretically and compared to HFSS simulation.

A uniform slotted SIW leaky-wave antenna is designed that has beam scanning from near broadside (though not exactly at broadside) to forward endfire (not exactly at endfire for a finite ground plane). This type of SIW leaky-wave antenna has a wide impedance bandwidth and a narrow beam that scans with frequency. When the antenna radiates not too close to endfire, it works as a leaky-wave antenna, and the radiation is mainly due to the leaky wave, which is fast wave. However, results show that when this antenna radiates near endfire, it becomes a surface-wave antenna since the radiation is mostly produced by a surface wave, which is slow wave. A prototype is fabricated, and measured results are consistent with the simulation and the theoretical results.

II. Theory

We show the geometry of the slotted SIW leaky-wave antenna in Fig. 1. Leakage is obtained by introducing a periodic set of transverse slots on the top of the SIW (between via centers), which interrupt the current flow on the top wall. The width of the SIW is w. The dielectric constant of the substrate is ε_r, and the thickness is h. The diameter of the vias is d, and the distance between adjacent vias is s. The length and width of the slots are L and W, and the period of the slots is p. For the slotted SIW investigated here, the structure has a small period p compared to the wavelength so that the antenna radiates from the dominant $n = 0$ space harmonic. To ensure a pure polarization, the slot width W is assumed small compared to the slot length L.

The SIW can be taken as a conventional dielectric-filled rectangular waveguide with an effective width w_{eff} [8]. The effective width w_{eff} can be approximately calculated from empirical formulas [5], [7], [8] and can also be accurately calculated from HFSS [6] and other numerical calculations [9]. For example, the effective width of the SIW shown in Fig. 1 is $w_{\text{eff}} = 9.9842$ mm, which is calculated from the empirical formulas in [7].

Since SIW can be taken as a conventional dielectric-filled rectangular waveguide, the slotted SIW can be analyzed as a dielectric-filled rectangular waveguide with transverse slots. Fortunately, the dispersion relations and modes for the transverse slotted rectangular waveguide with dielectric filling have been well investigated in [3]. Reference [3] gives equations for analyzing transverse slotted rectangular waveguide with an arbitrary dielectric filling, while [1] gives equations only for transverse slotted rectangular waveguide with air filling.

As assumed in [3], the tangential electric field in the zeroth slot on the SIW is assumed to be

$$\mathbf{E}_t = \underline{\hat{\mathbf{z}}} \cos(\pi x/L). \tag{1}$$

By enforcing an aperture magnetic field integral equation using a space-domain approach, the propagation wavenumber $k_z = \beta - j\alpha$ of the slotted rectangular waveguide can then be calculated from the following transcendental equation [3]:

$$\sum_{n=-\infty}^{\infty} \operatorname{sinc}^2(k_{zn}W/2) \left\{ \sum_{m=1,3,5,\ldots}^{\infty} \left[k_1^2 - \left(\frac{m\pi}{w_{\text{eff}}}\right)^2 \right] \cdot \frac{\cos^2\left(\frac{m\pi L}{2w_{\text{eff}}}\right)}{\left(1 - \frac{m^2L^2}{w_{\text{eff}}^2}\right)^2} \frac{\cot(k_{ymn1}h)}{k_{ymn1}h} + j\frac{\pi^2}{16} \cdot \frac{\mu_r w_{\text{eff}}}{L^2 h} \cdot I_n \right\} = 0 \tag{2}$$

where

$$I_n = \int_0^{\pi} \left[\left(k_0^2 \frac{L^2}{\pi^2} - 1 \right) (\pi - r)\cos(r) + \left(k_0^2 \frac{L^2}{\pi^2} + 1 \right) \sin(r) \right] \cdot H_0^{(2)} \left(\frac{k_{\rho n} L r}{\pi} \right) dr \tag{3}$$

and

$$k_{zn} = k_z + 2n\pi/p \tag{4}$$

$$k_{\rho n} = \sqrt{k_0^2 - k_{zn}^2} \tag{5}$$

$$k_{ymn1} = \sqrt{k_1^2 - (m\pi/w_{\text{eff}})^2 - k_{zn}^2}. \tag{6}$$

In (6) k_1 is the wavenumber in the substrate. If the substrate is a lossy dielectric with a loss tangent $\tan\delta$, k_1 is

$$k_1 = k_0\sqrt{\varepsilon_r(1 - j\tan\delta)}. \tag{7}$$

Note that $k_{\rho n}$ in (5) has two possible values due to the square root function. The choice $\operatorname{Im}(k_{\rho n}) > 0$ corresponds to an improper wave and causes the wave to be exponentially increasing with radial distance from the z-axis. The other choice $\operatorname{Im}(k_{\rho n}) < 0$ corresponds to a proper wave and causes the wave to be exponentially decaying with radial distance.

For a conventional rectangular waveguide with transverse slots, three types of modal solutions are found: a leaky improper waveguide mode, a bound (nonleaky) proper waveguide mode, and a surface-wave type of mode [3]. The leaky waveguide mode is an attenuated mode that typically dominates above the cutoff frequency of the TE_{10} mode in the closed rectangular waveguide. The proper waveguide mode is a bound mode that has no attenuation for a lossless structure (where the conductor and the dielectric are lossless). Both the leaky waveguide mode and proper waveguide mode have most of their power stored inside the waveguide and represent a perturbation of the closed waveguide (the former dominates in the fast-wave region, the latter in the slow-wave region). The surface-wave mode is also a proper bound wave, but this mode has most of its power stored at the surface of the waveguide and not inside the waveguide, so

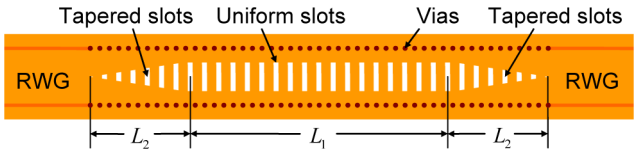

Fig. 2. Slotted SIW with rectangular waveguide feed. The SIW has the same dimensions as in Fig. 1. The width of the rectangular waveguide is $w_{\text{eff}} = 9.9842$ mm. The slots at both ends are linearly tapered. The length $L_1 = 180$ mm, $L_2 = 30$ mm.

this mode does not represent a perturbation of the closed rectangular waveguide. For the improper leaky waveguide mode, $k_{\rho n}$ is chosen so that the imaginary part of $k_{\rho n}$ is positive for $n = 0$ and negative for all other n. For the proper waveguide mode or the surface-wave mode solution, $k_{\rho n}$ is chosen so that the imaginary part of $k_{\rho n}$ is negative for all n. A more complete explanation for the modal analysis is given in [3].

III. Method to Extract Wavenumber From HFSS

In order to validate the wavenumber calculated theoretically from (2), we can extract the wavenumber by simulating a slotted SIW with HFSS. Here, we first simulate the structure shown in Fig. 2 and sample the near-field electric field along the uniform slotted SIW at a periodic distance p (the period of the slots). The tapered ends help to minimize unwanted end reflections, resulting in a more ideal field in the uniform region. To simplify the simulation, the slotted SIW is fed by a rectangular waveguide with a width that is the effective width of the SIW.

Suppose there are two traveling waves with wavenumbers k_{z1} and k_{z2} propagating inside the SIW, so that the field can be modeled using

$$E_y = A_1 e^{-k_{z1} z} + A_2 e^{-k_{z2} z}. \tag{8}$$

We use MATLAB to numerically fit these two traveling waves to the sampled near-field data obtained from HFSS, using a least-square criterion for determining the "best fit." For a bound-mode solution, we assume the wavenumber to be a real number. The procedure is illustrated in Fig. 3 at a frequency of 11.7 GHz, where we assume that there is a leaky mode with an unknown complex wavenumber k_{z1} and a surface-wave mode with a real wavenumber k_{z2} propagating inside the waveguide. Fig. 3 shows that the sum of the leaky mode and the surface-wave mode fits the near-field data from HFSS very well. At this frequency, the amplitude of the physical leaky mode is much stronger than the amplitude of the surface-wave mode, though the surface-wave mode causes a noticeable oscillation in the field plot.

Since the surface-wave mode has most of the fields outside (but near the surface) of the SIW, it is more accurate to sample the near field outside the SIW for determining the wavenumber of the surface-wave mode. For the leaky mode or proper waveguide mode, it is better to sample the electric field inside the SIW because these modes have most of the fields inside the SIW. Once the wavenumbers are known, the amplitudes of the modes in (8) can be found by sampling along a given line (the amplitudes of the modes depend on the location of the line). Since two modes (leaky mode and surface-wave mode) can simultaneously propagate along the slotted SIW when the antenna has

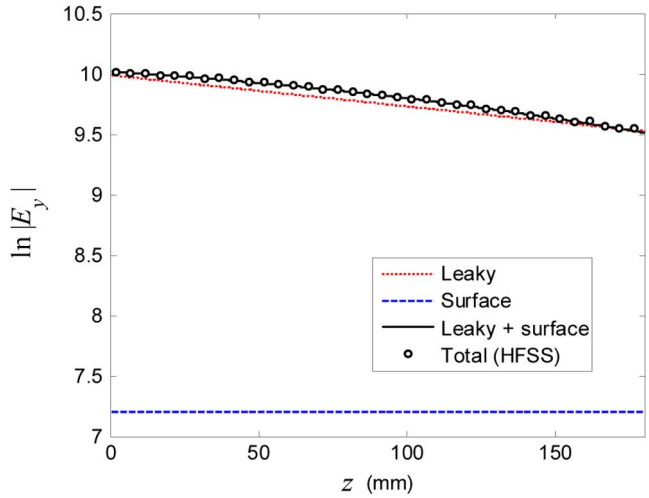

Fig. 3. Electric field inside the uniform slotted SIW. The antenna has the structure in Fig. 2. The slotted SIW has the same dimensions as in Fig. 1. The frequency is $f = 11.7$ GHz. The substrate and the conductor are lossless.

not yet scanned to endfire, in order to extract a more accurate result from HFSS, the length L_1 of the antenna shown in Fig. 2 should be relatively large. Here, we select the length of L_1 as 180 mm (about 7 wavelengths in free space).

For the leaky waveguide mode or the proper waveguide mode, a value that is close to the theoretical wavenumber from (2), or even the wavenumber of the closed equivalent rectangular waveguide, can be used as the initial guess for determining the final wavenumber in the least-squares solution. For the surface-wave mode, a value close to the wavenumber in free space can be used as the initial guess.

If we fit two traveling waves using expression (8) to the electric field at the slots obtained from HFSS simulation, we can also estimate the percentage of the leaky mode that is present in the total near field by using

$$P_{\text{LM}}^{\%} = 100\left(\frac{|A_1|^2}{|A_1|^2 + |A_2|^2}\right) \tag{9}$$

where we suppose the leaky mode is mode 1 and the surface-wave mode is mode 2, so A_1 represents the amplitude of the leaky mode and A_2 represents the amplitude of the surface-wave mode. The tangential electric field is sampled at the center of the slots in this calculation since this is the field that is responsible for radiation.

IV. Numerical Results

A. Dispersion Relations

We calculate the wavenumber for the equivalent rectangular waveguide ($w_{\text{eff}} = 9.9842$ mm) with transverse slots from (2) and show the normalized phase and attenuation constants in Figs. 4 and 5. From Fig. 4, we find that when the frequency is less than 11.98 GHz, the phase constant of the leaky mode is less than k_0, so the leaky mode is a fast wave and the solution is in the physical region. In this same frequency region, there is another solution that is proper with a zero attenuation constant. This proper mode is called a surface-wave type of mode because most of its power is outside the waveguide but close to

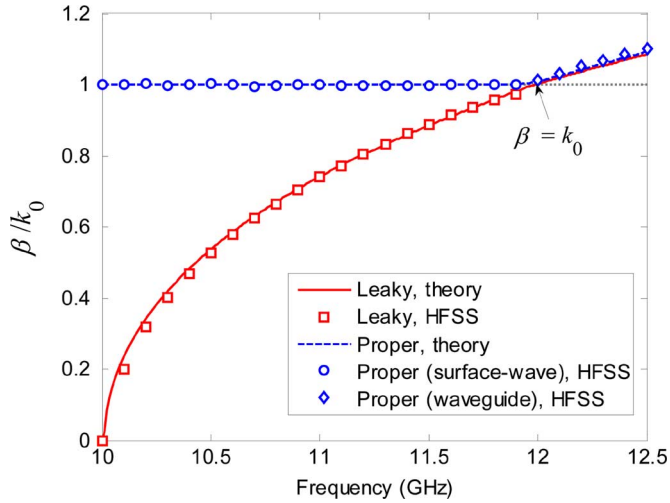

Fig. 4. Normalized phase constant in slotted SIW. The slotted SIW has the dimensions given in Fig. 1. The substrate and the conductors are lossless.

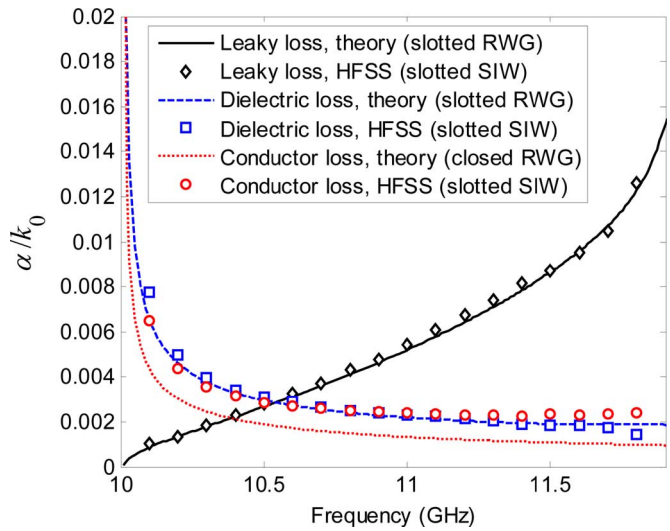

Fig. 5. Normalized attenuation constant in slotted SIW. The slotted SIW has the dimensions shown in Fig. 1. The lossy dielectric has $\tan\delta = 0.001$, and the lossy conductor has $\sigma = 5.8 \times 10^7$ S/m.

the surface [3]. When the frequency is larger than 11.98 GHz, the phase constant of the leaky mode is larger than k_0, so the leaky mode is a slow wave and it will lose physical significance. Beyond 11.98 GHz, a proper waveguide mode now also exists instead of a surface-wave mode, which has most of its power stored inside the waveguide.

We calculate the wavenumber of the modes in the slotted SIW from HFSS. By numerically fitting two traveling waves to the near-field electric field obtained from the HFSS simulation, we can extract the wavenumber of leaky wave and the other proper wave (either the surface-wave mode or the proper waveguide mode) [3].

We show the normalized phase and attenuation constants of the leaky mode in slotted SIW from HFSS simulation in Figs. 4 and 5 and compare with theoretical results for the slotted rectangular waveguide [from (2)]. From the phase constant shown in Fig. 4, we find that the simulated results for the slotted SIW

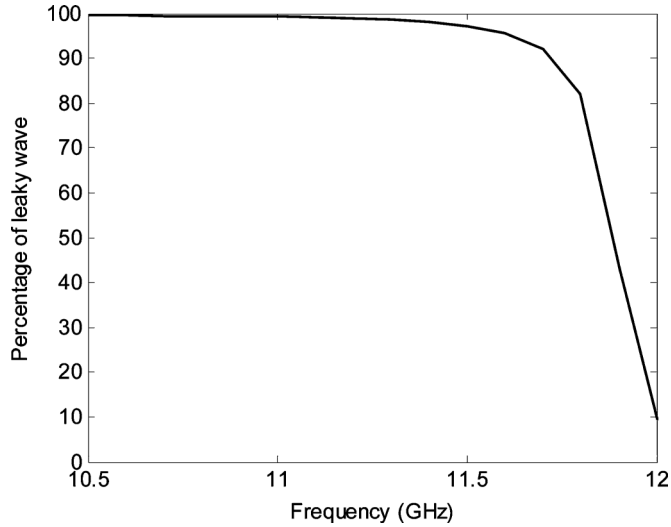

Fig. 6. Percentage of the leaky mode present in the slotted SIW. The dimensions are the same as in Fig. 4.

are very close to the theoretical results for the rectangular waveguide with transverse slots. In Fig. 5, the attenuation constant of the leaky mode in slotted SIW is very close to the theoretical results for slotted rectangular waveguide, so the leakage from the vias is very small compared to the leakage from the slots in the slotted SIW, and the slotted SIW can be taken as a slotted rectangular waveguide.

By numerically fitting two traveling waves to the near-field electric field on the slots obtained from the HFSS simulation, we can also estimate the percentage of the leaky mode that is present in the slotted SIW (the procedure is discussed in Section III). The percentage of the leaky mode is shown in Fig. 6. From Fig. 6, we find that at low frequency (when the antenna has not yet scanned to endfire), the leaky mode is the dominant mode. However, the percentage of the leaky mode decreases as the frequency increases because the surface-wave mode is excited more as the frequency increases. Also, even more importantly, as the frequency approaches toward the leaky-mode cutoff (11.98 GHz), the leaky mode loses physical significance rapidly, so the percentage of the leaky mode becomes very small.

B. Dielectric Loss

When loss is present, all modes have a complex wavenumber. For calculating the dielectric loss in slotted rectangular waveguide, we use the wavenumber k_1 from (7) in (2) to solve for the complex wavenumber of the proper and improper modes in the lossy slotted rectangular waveguide. This yields the attenuation constant $\alpha_l + \alpha_d$ that accounts for leakage and dielectric loss. We then calculate the attenuation constant α_l due to only leakage loss by using (2) with a real k_1. By subtracting α_l from $\alpha_l + \alpha_d$, we obtain the attenuation constant α_d due to dielectric loss. For the leaky-mode solution, the attenuation constant due to dielectric loss in slotted rectangular waveguide is included in Fig. 5. We also calculate the attenuation constant α_d for the leaky mode in slotted SIW from HFSS simulation and show the results in Fig. 5. In the HFSS simulation, we follow a similar

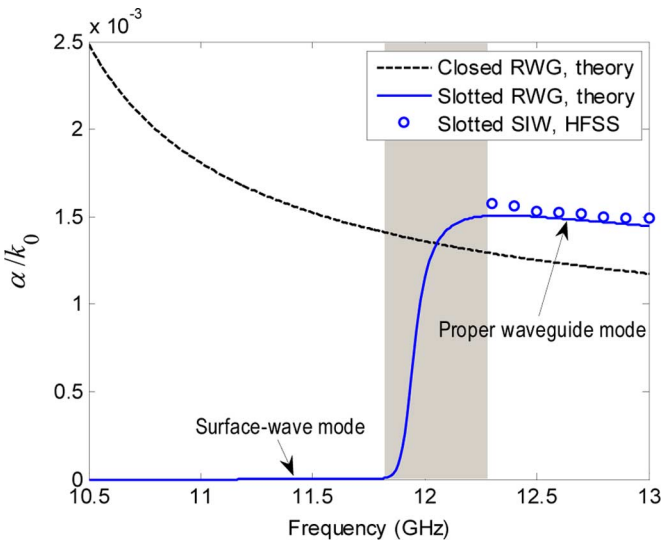

Fig. 7. Dielectric loss effect on the proper mode in slotted SIW. The slotted SIW has the dimensions shown in Fig. 1. The lossy dielectric has $\tan\delta = 0.001$.

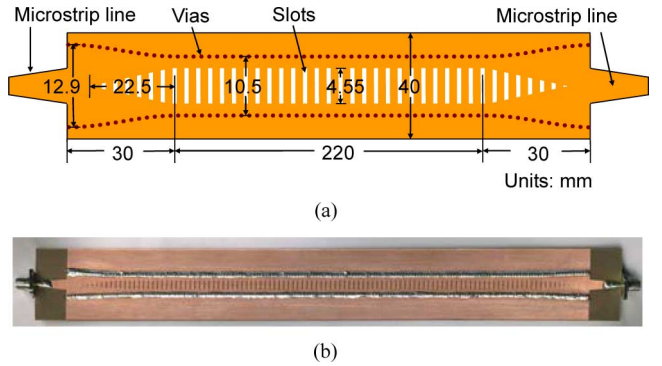

Fig. 8. Geometry of uniform slotted SIW leaky-wave antenna. The uniform portion of the slotted SIW has the same dimensions as in Fig. 1. The dielectric has a tangent loss of $\tan\delta = 0.001$, and the conductor has a conductivity of $\sigma = 5.8 \times 10^7$ S/m. The antenna is fed with a tapered microstrip line with a length of 15 mm and a width linearly varying from 4.7 to 3.1 mm. The length and width of the ground plane are 310.2 and 40 mm, respectively. (a) Geometry (not to scale). (b) Measured antenna.

procedure discussed above, in which we first simulate a structure that uses a lossy dielectric substrate to obtain $\alpha_l + \alpha_d$, and then subtract α_l that is obtained from the simulation of a lossless structure. Fig. 5 shows that the theoretical dielectric loss of rectangular waveguide with transverse slots agrees very well with the dielectric loss of slotted SIW from HFSS.

As shown in Fig. 7, the attenuation constant of the proper waveguide mode is not zero because of the dielectric loss. We show the dielectric loss in the slotted rectangular waveguide and compare to the dielectric loss in both the slotted SIW and the closed rectangular waveguide. Also included is the dielectric loss of the surface-wave mode, obtained theoretically. (The dielectric loss of the surface-wave mode is not easy to obtain from HFSS because the amplitude of this mode is very small in the region where the leaky mode is the dominant mode.) The dielectric loss of the surface-wave mode is very small because most of the power carried in this mode is outside the waveguide and not in the lossy substrate. When the surface-wave mode transitions to become the proper waveguide mode, the normalized attenuation constant is not close to zero any more, but becomes a little larger than the attenuation constant of the closed rectangular waveguide. Fig. 7 also shows that the results for the slotted SIW from HFSS are very close to the theoretical results for the slotted rectangular waveguide.

Fig. 7 indicates that the surface-wave mode is evolving into the proper waveguide mode in the region (shown shaded in Fig. 7) where the frequency is between 11.82 and 12.28 GHz. At the same time that the surface-wave mode evolves into the proper waveguide mode, the leaky waveguide mode loses its physical significance, and the waveguide mode is replaced by the proper waveguide mode [3] as the physical waveguide-like mode (though the improper leaky mode continues to exist). This corresponds to the region in Fig. 6 in which the percentage of leaky mode decreases sharply. The transition region from 11.82 to 12.28 GHz thus includes three modes: the leaky waveguide mode, the surface-wave mode, and the proper waveguide mode. The upper cutoff frequency of the leaky waveguide mode ($f = 11.98$ GHz) lies within this region.

C. Conductor Loss

To calculate the conductor loss of slotted SIW, we first use HFSS to simulate a slotted SIW with a lossy conductor and calculate the attenuation constant $\alpha_l + \alpha_c$ that includes leakage and conductor loss. Second, we simulate a slotted SIW that has perfect conductors to determine α_l that only includes leakage. Then, we subtract to get the attenuation constant α_c that is due to conductor loss.

We include the conductor loss of slotted SIW obtained from HFSS in Fig. 5. Since it is difficult to calculate theoretically the conductor loss in slotted rectangular waveguide or in slotted SIW, we only compare simulated results for slotted SIW with the conductor loss of a closed rectangular waveguide, calculated from [20]

$$\alpha_c = \frac{R_s}{w_{\text{eff}}^3 h k_0 \eta_0 \sqrt{k_0^2 \varepsilon_r - (\pi/w_{\text{eff}})^2}} (2h\pi^2 + h^3 k_0^2 \varepsilon_r). \tag{10}$$

This comparison shows that the conductor loss of slotted SIW is larger than the conductor loss of a corresponding closed rectangular waveguide. This is due to the fact that the current must bend around the slots, increasing the current density surrounding the slots, resulting in increased conductor loss. In fact, the conductor loss of slotted rectangular waveguide (not shown) is also larger than the conductor loss of closed rectangular waveguide for this same reason.

V. Uniform Slotted SIW Leaky-Wave Antenna

A. Geometry

The geometry of the uniform SIW leaky-wave antenna is shown in Fig. 8. The dominant part of this leaky-wave antenna is a uniform SIW with a series of uniform transverse slots, and this part has a length of 220 mm.

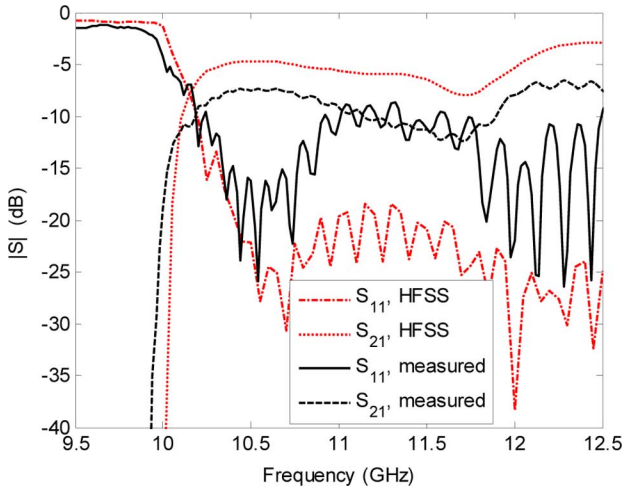

Fig. 9. S-parameters of the uniform slotted SIW leaky-wave antenna shown in Fig. 8. The antenna is with finite ground plane.

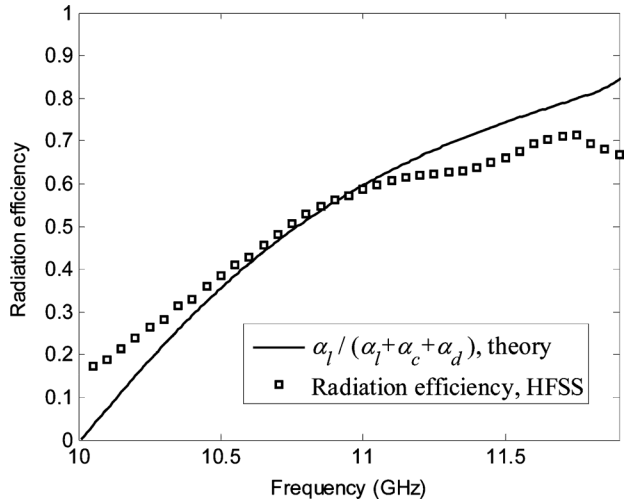

Fig. 10. Radiation efficiency for the slotted SIW antenna shown in Fig. 8. The antenna is with finite ground plane.

Since the slots cause a perturbation to the TE_{10} mode of the SIW [3], to suppress the reflection coefficient S_{11}, we taper the slots linearly at both ends as shown in Fig. 8. The length of the tapered part is 22.5 mm. We taper the slot length L from zero to 4.55 mm and keep the other parameters of the slots constant. To enhance the bandwidth, we taper the SIW width as a cosine function at both ends, as in [12]. The length of the tapered SIW section is 30 mm. We taper the width w of the SIW from 10.5 to 12.9 mm and keep the other parameters of the SIW constant. We use microstrip line to feed the SIW leaky-wave antenna. In order to obtain a better match between the input SIW and the microstrip line, we also linearly taper the microstrip line using the method described in [21].

B. S-Parameters

We use HFSS to simulate the structure shown in Fig. 8. The reflection coefficients are shown in Fig. 9 and compared to the measured data. The measured results for S_{11} are a little higher than the simulated results because the fabrication is not accurate enough and the loss from the SMA connectors is not included in the simulation. However, both results show that S_{11} is mostly less than -10 dB in the band of interest (from 10.2 to 12 GHz).

The measured data for S_{21} are a little lower than the simulated results, which might result from the increased S_{11} and probably the increased conductor loss in the measurement. A small shift of frequency is also observed between the simulated results and the measured data, probably due to a difference in the dielectric constant used in the experiment and some small errors in fabrication. Due to such errors, the propagation wavenumber in the fabricated antenna has a small shift compared to the simulated antenna. Nevertheless, the simulated results are close to the measured results. Both the measured and simulated results show that when the frequency is a little larger than 10.2 GHz, S_{21} is relatively high because the attenuation constant is small and most of the power is transmitted to the output end. However, as the frequency increases, S_{21} will decrease because the attenuation constant of the leaky mode increases, which leads to more power being radiated into space. Measured results show that S_{21} is lower than -10 dB in the band from 11.15 to 11.9 GHz, which indicates that most of the power is consumed (radiated and dissipated) by the antenna. However, as the frequency increases still further beyond the endfire point, S_{21} increases dramatically since the leaky mode is now becoming nonphysical and the proper waveguide mode is becoming the dominant mode, which has very little attenuation (due only to conductor and dielectric loss).

C. Radiation Efficiency

We estimate the radiation efficiency e_r of slotted rectangular waveguide from

$$e_r = \frac{\alpha_l}{\alpha_l + \alpha_d + \alpha_c} \tag{11}$$

where the sum of the leakage loss α_l and the dielectric loss α_d can be calculated from (2) and the conductor loss can be calculated from (10). We show the radiation efficiency of slotted rectangular waveguide calculated this way in Fig. 10. In Fig. 10, we also show the radiation efficiency of the slotted SIW antenna obtained directly from HFSS by simulating the structure shown in Fig. 8. Note that the radiation efficiency obtained from HFSS is not the total efficiency because the HFSS radiation efficiency calculated here does not take the mismatch or the power absorbed in the load port into account. This is done to agree with the definition used in (11). At a frequency that is close to the cutoff frequency of the SIW (10 GHz), the theoretical radiation efficiency is lower than the simulated one from HFSS because there is another radiation mechanism due to the connection between the microstrip line and the SIW. When the frequency increases and the frequency is lower than the upper cutoff frequency of the leaky mode, the theoretical results from (11) are a little higher than the radiation efficiency calculated from HFSS because the conductor loss of closed rectangular waveguide calculated from (10) is smaller than the conductor loss of the slotted SIW, and the material loss (conductor loss and dielectric loss) of the feeding structure is not included in the theoretical calculation. Nevertheless, the theoretical results are close to the radiation efficiency from HFSS. When the frequency is larger than the upper cutoff frequency of the leaky mode, the leaky

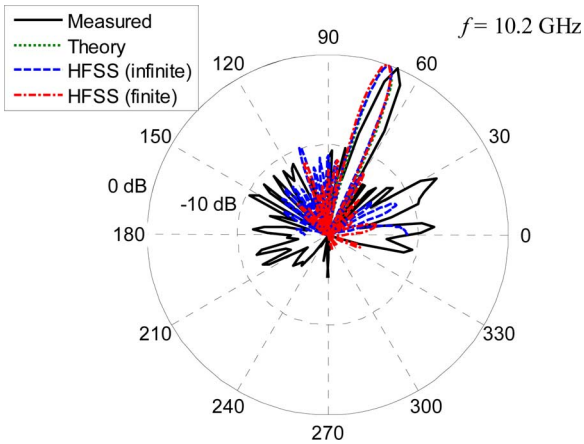

Fig. 11. Radiation patterns for the structure shown in Fig. 8 at 10.2 GHz.

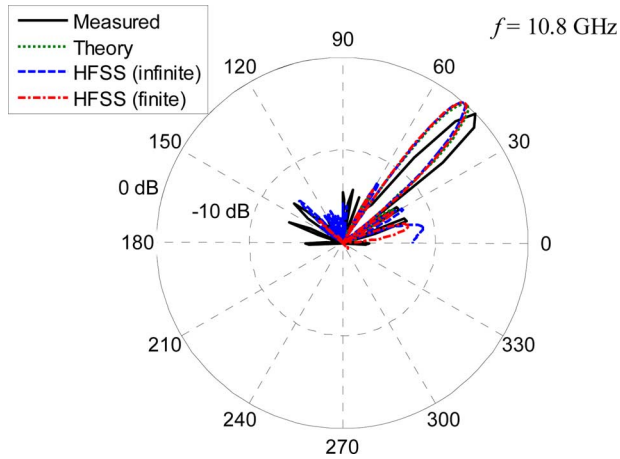

Fig. 12. Radiation patterns for the structure shown in Fig. 8 at 10.8 GHz.

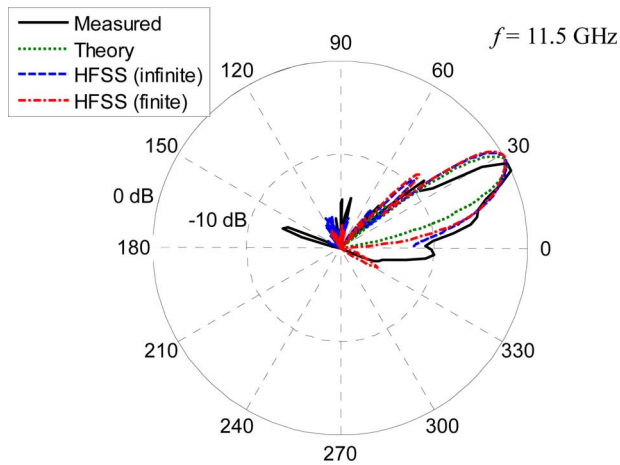

Fig. 13. Radiation patterns for the structure shown in Fig. 8 at 11.5 GHz.

mode loses physical significance, and the radiation efficiency of the slotted SIW becomes lower than the theoretical results from (11).

D. Radiation Patterns

We show the normalized radiation patterns in Figs. 11–14. It is seen that the measured results are very close to the simulated patterns for the antenna with a finite ground plane, although a small discrepancy for the radiation angle due to a shift of frequency is observed. The main beam of the antenna can scan from near broadside to near endfire as frequency increases. When the antenna is radiating near broadside the radiation efficiency is rather poor due to the smaller leakage attenuation and increased attenuation due to material loss. However, as the antenna scans in the forward quadrant, the radiation efficiency increases.

In the theoretical calculation, we use the theoretical wavenumber from (2) and calculate the normalized radiation pattern by

$$E_\theta(\theta) = E_0 \sum_{n=1}^{N} L_n e^{-jk_z z_n} e^{jk_0 z_n \cos\theta} \qquad (12)$$

where L_n is the length of the nth slot in Fig. 8. In the theoretical calculation for the wavenumber k_z, the leaky loss and the dielectric loss are accounted for, but the conductor loss is not included because it is difficult to calculate the conductor loss of slotted SIW theoretically.

In the theoretical calculation, when the antenna has not yet scanned to endfire, we use the theoretical wavenumber for the leaky mode to calculate the pattern from (12). Figs. 11–13 show that the theoretical results that assume a leaky mode are very close to the main beam of the simulated results from HFSS, which means this antenna works as a leaky-wave antenna when the antenna has not yet scanned to endfire. When the antenna has not yet scanned to endfire, the radiation is mainly produced by the leaky mode and the phase constant of the leaky mode is less than k_0, so the antenna works as a fast-wave (leaky-wave) radiator.

In Fig. 12, the simulated pattern for the antenna with infinite ground plane has a sidelobe at endfire that is due to the surface-wave radiation. This sidelobe is not observed in the theoretical calculation because the surface-wave mode is not included in the theoretical calculation. The surface-wave mode has a wavenumber only slightly larger than the wavenumber of free space, so the surface-wave mode can only radiate at endfire and contaminates the leaky-wave radiation pattern. For the antenna with a finite ground plane, the sidelobe due to the surface-wave mode is radiating at near endfire because of finite ground plane diffraction effects. In the measured patterns, the sidelobe due to the surface wave is also observed near endfire. The surface-wave mode is excited stronger as frequency increases. Hence, at low frequency, the sidelobe due to the surface-wave mode is not pronounced, as shown in Fig. 11. As frequency increases, the leaky mode scans very close to endfire, and the main beam of the leaky mode becomes very close to the main beam of the surface-wave mode. Therefore, the main beam of the leaky mode becomes merged into that of the surface-wave mode, as shown in Fig. 13. Note that in Fig. 13, the radiation pattern calculated from theory only accounts for the leaky mode, so no merging for the leaky-mode pattern into a surface-wave pattern is observed.

In Fig. 14, we show the theoretical radiation pattern that assumes a leaky mode and compare to the simulated results and

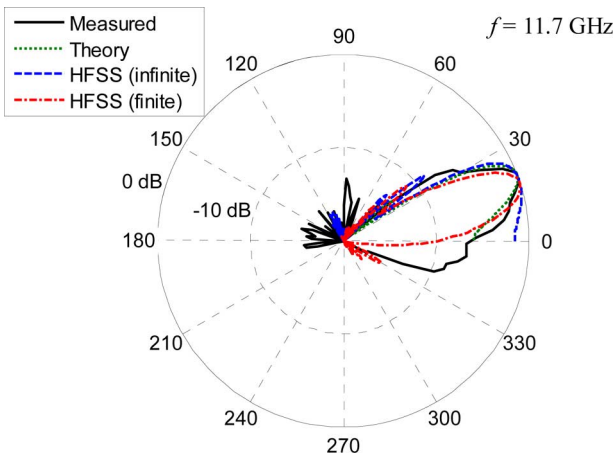

Fig. 14. Radiation patterns for the structure shown in Fig. 8 at 11.7 GHz.

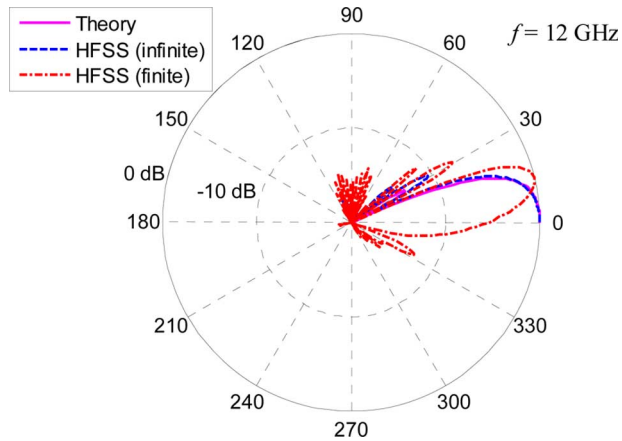

Fig. 15. Simulated and theoretically calculated radiation patterns for the antenna shown in Fig. 8 at 12 GHz.

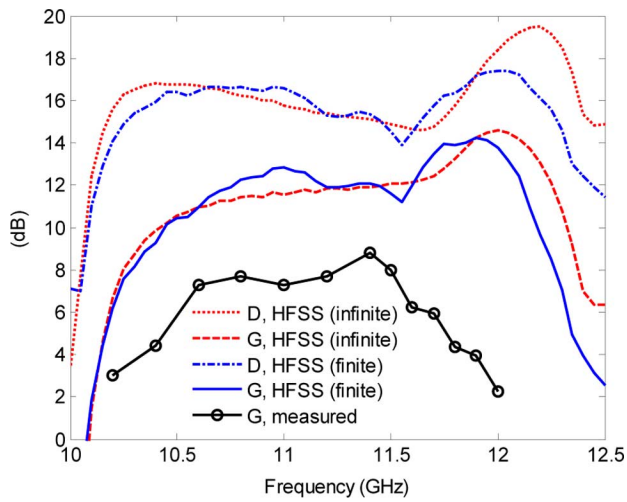

Fig. 16. Directivity and gain of the uniform slotted SIW leaky-wave antenna shown in Fig. 8.

measured results at a frequency of 11.7 GHz. It appears the theoretical leaky-wave pattern agrees well with the measured results. However, since a shift of frequency (about 0.15-GHz shift at a frequency of 11.7 GHz) exists between the measured result and the theoretical one, the theoretical frequency corresponding to the measured antenna at 11.7 GHz should be chosen to be about 11.85 GHz. As discussed before in connection with Figs. 6 and 7, the percentage of the leaky mode is not very large and the surface-wave mode is transitioning into the proper waveguide mode at 11.85 GHz, so the measured pattern should actually be composed of a leaky mode and a mode that is somewhat between the surface-wave mode and the proper waveguide mode. The measured antenna appears to suffer more from finite ground plane diffraction effects than does the antenna simulated in HFSS. Therefore, owing to the serious finite ground plane diffraction effects, the measured main beam is not so close to endfire and by coincidence agrees well with the simulated antenna even though a small shift of frequency exists. Because of the finite ground plane diffraction effects, the practical antenna cannot scan to exactly endfire.

In Fig. 15, we show the simulated results for the antenna working as a slow-wave (surface-wave) antenna at 12 GHz. Also included is the radiation pattern calculated theoretically by (12). Note that in the theoretical calculation by (12), the wavenumber k_z should be the one for the surface-wave or proper waveguide mode (the two are essentially coincident at this frequency) because at this frequency the leaky mode is not the dominant mode any more as shown in Fig. 6. Fig. 15 shows that the theoretical results agree very well with the simulated results for the antenna with an infinite ground plane. In fact, the theoretical result that assumes a leaky mode (not shown) is not so close to the simulated results. Since the proper mode (surface-wave mode or proper waveguide mode) is a slow-wave mode, the antenna works as a slow-wave antenna at this frequency. Fig. 15 shows that the simulated radiation pattern for the antenna with a finite ground plane is not radiating exactly at endfire due to finite ground plane diffraction. At endfire, the pattern for the finite ground plane case is lower than the same pattern at the beam peak by about 6 dB, a result that is consistent with the geometrical theory of diffraction (GTD). (GTD predicts a 6-dB drop at endfire for a finite ground plane, regardless of the ground plane size.) Using a larger ground plane should help to minimize the finite ground plane diffraction effects. Here we do not show the measured results because the gain of the measured radiation pattern is rather poor due to the shift of frequency and the more serious finite ground diffraction effects.

E. Gain and Directivity

Fig. 16 shows the measured gain for the practical antenna and the simulated gains for the antennas with a finite ground plane and with an infinite ground plane. The shape of the measured result is very similar to the simulated ones (realized gains), although the measured gain is lower than the simulated gains. When the frequency is larger than the cutoff frequency of the SIW (10.2 GHz), the gain increases as the frequency increases because the leakage constant (attenuation constant due to radiation) increases as the frequency increases, and hence more power is radiated into space instead of being absorbed at the output termination. As the frequency increases even more, the measured gain and the simulated gain for the antenna with a

finite ground plane decrease a little bit, probably due to an increase of the beamwidth. When the frequency increases still further, the gains drop sharply because the main beam passes endfire and more power is transmitted to the terminating end instead of being radiated into space. As the frequency approaches cutoff (about 10 GHz) the attenuation due to material loss increases dramatically (see Fig. 5). While material loss does not directly affect the directivity (only the gain), the increased material loss results in an increased overall attenuation constant for the leaky mode, and this in turn lowers the size of the effective radiating aperture, which lowers the directivity. The gain is lowered even more due to the decreased radiation efficiency associated with the increased material loss.

There are several reasons conjectured for the measured gain being lower than the simulated gain. First, the loss from the SMA connector that is not included in the simulation and some errors in fabrication result in a higher S_{11}, which also decreases the measured gain. Second, the conductor loss and dielectric loss in the fabricated antenna are probably higher than that in the simulated one (especially the conductor loss). In the fabricated antenna, the vias are replaced by tinned pins, which might lead to an increased conductor loss. This also results in a lower S_{21}. Third, the chamber for measuring the antenna is not ideally large enough for the length of the antenna measured here, which would lead to some inaccuracy for the gain measurement. As a matter of fact, a similar discrepancy between the simulated results and measured results for another SIW leaky-wave antenna is also observed in [15], and the reasons discussed above were also mentioned in [15]. In our case, another discrepancy is also observed. The measured antenna reaches the highest gain at about 11.4 GHz, while the simulated antenna with a finite ground plane reaches the highest gain at about 11.9 GHz. This is because a small shift of frequency exists due to fabrication, and the measured antenna also suffers a more serious finite ground plane diffraction effect than the simulated one. Comparing the simulated gains for the antenna with a finite ground plane and the antenna with an infinite ground plane, it is also found that the finite ground plane diffraction effects would cause the gain of the antenna with a finite ground plane to drop at a lower frequency compared to the antenna with an infinite ground plane.

The simulated directivity and gain for the antenna with an infinite ground plane is also shown in Fig. 16 as a function of frequency. Fig. 16 shows that when the frequency is larger than 10.2 GHz, the directivity decreases as a function of frequency because the beamwidth increases as the scan angle θ goes from broadside to endfire (see [3]). However, when the frequency goes to about 11.7 GHz and the beam approaches endfire, the radiation pattern will change from a conical beam to a pencil beam, so the directivity will increase. The beam reaches endfire at about 11.9 GHz though the directivity continues to increase until about 12.2 GHz since the beam continues to narrow for a while as the beam scans beyond endfire where the phase constant is a little larger than k_0. At 12.2 GHz, the antenna works as a slow-wave antenna since $\beta > k_0$. According to the Hansen–Woodyard maximum directivity condition [22], [23], the largest directivity will occur when $\beta = k_0 + 2.94/L_1$ for $L_1 \gg \lambda_0$ and $\alpha = 0$, where L_1 is the antenna length. Although the Hansen–Woodyard condition assumes $\alpha = 0$ (a uniform aperture illumination), this condition is approximately valid for narrow-beam leaky-wave antennas [24]. From HFSS simulation, we find that at 12.2 GHz the phase constant of the uniform slotted SIW is $\beta = 1.0534\,k_0$, which is very close to the Hansen–Woodyard maximum directivity condition $\beta = 1.0523\,k_0$, corresponding to $L_1 \approx 220$ mm. Note that the directivity does not take into account the power lost at the terminating load port, and this explains why the shape of the gain and directivity curves are a bit different, and the fact that the gain curves peaks at a lower frequency than do the directivity curves.

The simulated directivity and gain for the antenna with a finite ground plane are also shown in Fig. 16. When the antenna has not yet scanned to endfire, the simulated directivity and gain for the finite ground plane antenna are very close to those for the antenna with an infinite ground plane. However, when the antenna scans to endfire, the simulated directivity and gain for the antenna with the finite ground plane start to drop at lower frequencies compared to the antenna with an infinite ground plane (due to the finite ground plane diffraction effects). After the antenna reaches endfire, the gain begins to drop sharply because the fields are evolving into the proper waveguide mode, and more power is transmitted into the terminating end instead of being radiated into space.

VI. Conclusion

A novel slotted SIW leaky-wave antenna is proposed that has the advantages of both rectangular waveguide with transverse slots and SIW. This structure supports a leaky mode, a proper waveguide mode, and a surface-wave mode, depending on the frequency region. The wavenumber of these waves was calculated theoretically and also evaluated by HFSS simulation. The leakage loss, dielectric loss, and conductor loss were evaluated by theory and from HFSS simulation. One of the advantages of this type of leaky-wave antenna is that it can scan to endfire. When the beam is scanned not too close to endfire, the pattern is due to the dominant leaky mode, as expected. However, as the beam is scanned to endfire, the structure acts as a slow-wave type of antenna, with the radiation coming from a combination of the proper waveguide mode and the surface-wave mode. Beyond endfire, the radiation mainly comes from the proper waveguide mode. Excellent agreement is obtained among the theoretical results, simulated results, and measured data.

Acknowledgment

The authors wish to acknowledge the China Scholarship Council (CSC) for awarding J. Liu a scholarship to study in the U.S. The authors also wish to acknowledge the following persons: V. R. Komanduri from the University of Houston, Houston, TX, for assistance in the theoretical research; Y. Li and X. Tang from Sun Yat-sen University, Guangzhou, China, for assistance in the experiment and measurement; and Y. Wu from Guangdong University of Technology, Guangzhou, China, for assistance with the measurements. The authors also wish to thank the reviewers for useful suggestions that have helped to improve this paper.

REFERENCES

[1] R. F. Hyneman, "Closely-spaced transverse slots in rectangular waveguide," *IRE Trans. Antennas Propag.*, vol. AP-7, no. 4, pp. 335–342, Oct. 1959.

[2] V. H. Rumsey, "Traveling wave slot antennas," *J. Appl. Phys.*, vol. 24, pp. 1358–1365, Nov. 1953.

[3] J. Liu, D. R. Jackson, and Y. Long, "Modal analysis of dielectric-filled rectangular waveguide with transverse slots," *IEEE Trans. Antennas Propag.*, vol. 59, no. 9, pp. 3194–3203, Sep. 2011.

[4] D. Deslandes and K. Wu, "Design consideration and performance analysis of substrate integrated waveguide components," in *Proc. 32nd Eur. Microw. Conf.*, Milan, Italy, Sep. 2002, vol. 2, pp. 881–884.

[5] Y. Cassivi, L. Perregrini, P. Arcioni, M. Bressan, K. Wu, and G. Conciauro, "Dispersion characteristics of substrate integrated rectangular waveguide," *IEEE Microw. Wireless Compon. Lett.*, vol. 12, no. 9, pp. 333–335, Sep. 2002.

[6] F. Xu and K. Wu, "Numerical multimode calibration technique for extraction of complex propagation constants of substrate integrated waveguide," in *Proc. IEEE MTT-S Int. Symp.*, June 2004, vol. 2, pp. 1229–1232.

[7] L. Yan, W. Hong, K. Wu, and T. J. Cui, "Investigations on the propagation characteristics of the substrate integrated waveguide based on the method of lines," *Proc. Inst. Elect. Eng., Microw. Antennas Propag.*, vol. 152, pp. 35–42, Feb. 2005.

[8] F. Xu and K. Wu, "Guided-wave and leakage characteristics of substrate integrated waveguide," *IEEE Trans. Microw. Theory Tech.*, vol. 53, no. 1, pp. 66–73, Jan. 2005.

[9] D. Deslandes and K. Wu, "Accurate modeling, wave mechanisms, and design considerations of a substrate integrated waveguide," *IEEE Trans. Microw. Theory Tech.*, vol. 54, no. 6, pp. 2516–2526, Jun. 2006.

[10] D. Deslandes and K. Wu, "Substrate integrated waveguide leaky-wave antenna: Concept and design considerations," in *Proc. Asia–Pacific Microw. Conf.*, Dec. 2005, pp. 346–349.

[11] F. Xu, K. Wu, and X. Zhang, "Periodic leaky-wave antenna for millimeter wave applications based on substrate integrated waveguide," *IEEE Trans. Antennas Propag.*, vol. 58, no. 2, pp. 340–347, Feb. 2010.

[12] J. Xu, W. Hong, H. Tang, Z. Kuai, and K. Wu, "Half-mode substrate integrated waveguide (HMSIW) leaky-wave antenna for millimeter-wave applications," *IEEE Antenna Wireless Propag. Lett.*, vol. 7, pp. 85–88, 2008.

[13] Y. J. Cheng, W. Hong, K. Wu, and Y. Fan, "Millimeter-wave substrate integrated waveguide long slot leaky-wave antennas and two-dimensional multibeam applications," *IEEE Trans. Antennas Propag.*, vol. 59, no. 1, pp. 40–47, Jan. 2011.

[14] Y. Dong and T. Itoh, "Composite right/left-handed substrate integrated waveguide leaky-wave antennas," in *Proc. Eur. Microw. Conf.*, Rome, Italy, Sep. 2009, pp. 276–279.

[15] Y. Dong and T. Itoh, "Composite right/left-handed substrate integrated waveguide and half mode substrate integrated waveguide leaky-wave structures," *IEEE Trans. Antennas Propag.*, vol. 59, no. 3, pp. 767–775, Mar. 2011.

[16] Y. Cheng, W. Hong, and K. Wu, "Millimeter-wave half mode substrate integrated waveguide frequency scanning antenna with quadri-polarization," *IEEE Trans. Antennas Propag.*, vol. 58, no. 6, pp. 1848–1855, Jun. 2010.

[17] G. M. Zelinski, G. A. Thiele, M. L. Hastriter, M. J. Havrilla, and A. J. Terzuoli, "Half width leaky wave antennas," *Microw. Antennas Propag.*, vol. 1, no. 2, pp. 341–348, Apr. 2007.

[18] Q. Lai, W. Hong, Z. Kuai, Y. Zhang, and K. Wu, "Half-mode substrate integrated waveguide transverse slot array antennas," *IEEE Trans. Antennas Propag.*, vol. 57, no. 4, pp. 1064–1072, Apr. 2009.

[19] M. Ohira, A. Miura, and M. Ueba, "60-GHz wideband substrate-integrated-waveguide slot array using closely spaced elements for planar multisector antenna," *IEEE Trans. Antennas Propag.*, vol. 58, no. 3, pp. 993–998, Mar. 2009.

[20] D. M. Pozar, *Microwave Engineering*, 2nd ed. New York: Wiley, 1998, p. 125.

[21] D. Deslandes and K. Wu, "Integrated microstrip and rectangular waveguide in planar form," *IEEE Microw. Wireless Compon. Lett.*, vol. 11, no. 2, pp. 68–70, Feb. 2001.

[22] W. L. Stutzman and G. A. Thiele, *Antenna Theory and Design*, 2nd ed. New York: Wiley, 1998.

[23] A. Sutinjo, M. Okoniewski, and R. H. Johnson, "Radiation from fast and slow traveling waves," *IEEE Antennas Propag. Mag.*, vol. 50, no. 4, pp. 175–181, Aug. 2008.

[24] E. M. O'Connor, D. R. Jackson, and S. A. Long, "Extension of the Hansen–Woodyard condition for endfire leaky-wave antennas," *IEEE Antennas Wireless Propag. Lett.*, vol. 9, pp. 1202–1204, 2010.

Juhua Liu was born in Heyuan, China, in 1981. He received the B.S. and Ph.D. degrees in electrical engineering from Sun Yat-sen University, Guangzhou, China, in 2004 and 2011, respectively.

From 2008 to 2009, he was a Visiting Scholar with the Department of Electrical and Computer Engineering, University of Houston, Houston, TX. His present research interests include microstrip antennas, substrate integrated waveguide antennas, leaky-wave antennas, periodic structures, and computational electromagnetics.

David R. Jackson (S'83–M'84–SM'95–F'99) was born in St. Louis, MO, in 1957. He received the B.S.E.E. and M.S.E.E. degrees from the University of Missouri, Columbia, in 1979 and 1981, respectively, and the Ph.D. degree in electrical engineering from the University of California, Los Angeles, in 1985.

From 1985 to 1991, he was an Assistant Professor with the Department of Electrical and Computer Engineering, University of Houston, Houston, TX. From 1991 to 1998, he was an Associate Professor in the same department, and since 1998 he has been a Professor with the department. His present research interests include microstrip antennas and circuits, leaky-wave antennas, leakage and radiation effects in microwave integrated circuits, periodic structures, and electromagnetic compatibility and interference.

Prof. Jackson is presently serving as the Chair of the Distinguished Lecturer Committee of the IEEE AP-S Society and is a Member-at-Large for U.S. Commission B of URSI (the International Union of Radio Science). He also serves as the chair of the MTT-15 (Microwave Field Theory) Technical Committee. He is on the Editorial Board for the IEEE TRANSACTIONS ON MICROWAVE THEORY AND TECHNIQUES. Previously, for the IEEE AP-S Society, he has been the Chair of the Transnational Committee, the Chapter Activities Coordinator, a Distinguished Lecturer, and a member of the AdCom. He was an Associate Editor for the IEEE TRANSACTIONS ON ANTENNAS AND PROPAGATION. He also previously served as the Chair of U.S. Commission B of URSI. He has also served as an Associate Editor for *Radio Science* and the *International Journal of RF and Microwave Computer-Aided Engineering*.

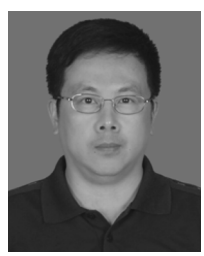

Yunliang Long (M'01–SM'02) was born in Chongqing, China, in 1963. He received the B.Sc., M.Eng., and Ph.D. degrees in electrical engineering from the University of Electronic Science and Technology of China (UESTC), Chengdu, China, in 1983, 1989, and 1992, respectively.

From 1992 to 1994, he was a Postdoctoral Research Fellow, then employed as an Associate Professor, with the Department of Electronics, Sun Yat-sen University, Guangzhou, China. From 1998 to 1999, he was a Visiting Scholar with the IHF, RWTH University of Aachen, Aachen, Germany. From 2000 to 2001, he was a Research Fellow with the Department of Electronics Engineering, City University of Hong Kong, Hong Kong. Currently, he is a Professor and the Head of the Department of Electronics and Communication Engineering, Sun Yat-sen University. He has authored and coauthored over 130 academic papers. His research interests include antennas and propagation theory, EM theory in inhomogeneous lossy medium, computational electromagnetics, and wireless communication applications.

Prof. Long is a member of the Committee of Microwave Society of CIE and is on the Editorial Board of the *Chinese Journal of Radio Science*. He is Vice Chairman of the Guangzhou Electronic Industrial Association. His name is listed in *Who's Who in the World*.